International Journal of Multiphase Flow xxx (2014) xxx–xxx

Contents lists available at ScienceDirect

International Journal of Multiphase Flow

journal homepage: www.elsevier.com/locate/ijmulflow

Two- and three-phase horizontal slug flow simulations using an interface-capturing compositional approach

Dimitrios Pavlidis [a,*], Zhihua Xie [a,c], James R. Percival [a], Jefferson L.M.A. Gomes [b], Christopher C. Pain [a], Omar K. Matar [c]

[a] Applied Modelling and Computation Group, Dept. of Earth Science and Engineering, Imperial College London, UK
[b] Environmental and Industrial Fluid Mechanics Group, School of Engineering, University of Aberdeen, UK
[c] Dept. of Chemical Engineering, Imperial College London, UK

ARTICLE INFO

Article history:
Received 16 April 2014
Received in revised form 16 July 2014
Accepted 20 July 2014
Available online xxxx

Keywords:
Implicit large-eddy simulation
Interface capturing
Slug flow
Three-phase flow

ABSTRACT

Progress on the development of a general framework for the simulation of turbulent, compressible, multi-phase, multi-material flows is described. It is based on interface-capturing and a compositional approach in which each component represents a different phase/fluid. It uses fully-unstructured meshes so that the latest mesh adaptivity methods can be exploited. A control volume-finite element mixed formulation is used to discretise the equations spatially. This employs finite-element pairs in which the velocity has a linear discontinuous variation and the pressure has a quadratic continuous variation. Interface-capturing is performed using a novel high-order accurate compressive advection method. Two-level time stepping is used for efficient time-integration, and a Petrov–Galerkin approach is used as an implicit large-eddy simulation model. Predictions of the numerical method are compared against experimental results for a five-material collapsing water column test case. Results from numerical simulations of two- and three-phase horizontal slug flows using this method are also reported and directions for future work are also outlined.

Introduction

It is well-known that the flow of water, oil and gas is of considerable practical importance for the oil and gas industry, occurring frequently during oil extraction, transportation, and flow-assurance applications. The physics of such flows involves the strong coupling of a number of mechanisms that include the interaction between the various phases, turbulence, viscosity- and density-contrast-driven instabilities, viscous and gravitational forces. This physics gives rise to complex dynamics that manifests itself through the formation of a wide range of phenomena such as interfacial waves, bubble and droplet creation, re-deposition, and entrapment, which has a direct bearing on the development of different flow regimes.

Bearing in mind that even two-phase gas–liquid flows exhibit complex dynamics, it is immediately apparent that the addition of a third phase will substantially add to this complexity. In such flows, physical phenomena additional to those occurring in two-phase flow play a crucial role. A major difference between two- and three-phase flow is due to the fact that in the latter, the presence of two liquids gives rise to a wider variety of flow patterns (Hall, 1997). Yet three-phase flow of two liquids and gas occurs often, especially in the production of hydrocarbons from oil and gas fields when oil, water, and natural gas flow in the transporting pipelines. The prediction of three-phase gas/liquid/liquid flows is therefore of industrial importance. In two- and three-phase flows, a frequently encountered flow regime is slug flow.

Even in two-phase flows (e.g. gas–liquid flows, for instance) in horizontal and inclined pipes, the generation and evolution of slugs in the slug-flow regime remains relatively poorly understood (Fabre and Line, 1992; King et al., 1998; Ujang et al., 2006). In these flows, the entrainment of gas from the large bubble to form small bubbles in the liquid slug is an important flow feature; the latter process is controlled by micro-scale capillary physics. Since the rate of creation of small bubbles is proportional to the pipe diameter cubed, the gas void fractions in bubble and slug flows converge with increasing pipe diameter. This has led to the observation that there is no 'classical' slug flow in large diameter pipes (Omebere-Iyari et al., 2007).

There are models of slug flow of increasing levels of complexity ranging from one assuming no bubbles (de Cachard and Delhaye, 1996) in the liquid slug (very small diameter pipes/very viscous

* Corresponding author.
E-mail address: dimitrios.pavlidis@imperial.ac.uk (D. Pavlidis).

http://dx.doi.org/10.1016/j.ijmultiphaseflow.2014.07.007
0301-9322/

liquids), to those with 29 equations (Fernandes et al., 1983). The first gives reasonable results either in the absence of bubbles, or if the gas fraction of gas in the slug is specified. More than often not, however, flows in hydrocarbon production pipelines are three-phase (oil–water–gas) rather than two-phase, and this additional complexity must be accounted for by any numerical method that aims to provide accurate and reliable predictions of these flows.

In this study, a novel method for detailed modelling of the physical processes that arise in complex multi-phase flows such as slug flows is proposed. The method is based on a multi-component approach that embeds information on interfaces into the continuity equations. A control volume-finite element method mixed formulation is used to discretise the spatial derivatives of the governing equations based on the P_1DG-P_2 (element-wise linear velocity, discontinuous between elements and element-wise quadratic pressure, continuous between elements, with C1 continuity everywhere) element pair (Cotter et al., 2009a; Cotter et al., 2009b). A novel interface-capturing scheme based on high-order accurate compressive advection methods is also used. This involves a down-winding scheme formulated using a high-order finite-element method to obtain fluxes on the control volume boundaries. These fluxes are subject to flux-limiting using a normalised variable diagram approach (Leonard, 1991; Darwish, 1993; Darwish and Moukalled, 2003) to obtain bounded and compressive solutions for the interface; this is essentially equivalent to introducing negative diffusion into the advection equation. The approach also uses a novel two-level time stepping method which allows large time steps to be used while maintaining stability and boundedness. Finally, a non-linear Petrov–Galerkin method is used as an implicit large-eddy simulation model.

This approach is able to simulate highly turbulent multi-phase flows of arbitrary number of phases and equations of state (density, pressure, temperature/internal energy relation), that can naturally represent phase change. The advantages of this approach are that the model is designed for compressible multi-fluid flows with an arbitrary number of fluids/materials, and does not rely on a priority list of materials (common for traditional multi-material models), which often produces spurious solutions (Wilson, 2009). In addition, the component advection equations are embedded into both pressure and continuity equations resulting in local mass balance (within each control volume).

Numerical predictions for the five-material collapsing water column test case are validated against experimental data. Results from numerical simulations of two-dimensional, two- and three-phase horizontal slug flows are then presented. A comparison of these results with experimental observations reveals good agreement and provides an indication of the accuracy, reliability, and efficiency of the numerical approach.

The remainder of this paper is organised as follows. A detailed description of the model is given in Section 'Methodology'. The model evaluation for the five-material collapsing water column test case is presented in Section 'Method validation: collapsing water column test case'. Two- and three-phase horizontal slug flow simulation results are presented in Sections 'Numerical simulation of two-phase horizontal slug flow' and 'Numerical simulation of three-phase horizontal slug flow', respectively. Finally, concluding remarks and directions for future work are given in Section 'Conclusions'.

Methodology

In multi-component flows, a number of components exist in one or more phases. In the present work, one phase is assumed, however, this is easily generalised to an arbitrary number of phases or fluids. For each fluid component i, the conservation of mass is defined as:

$$\frac{\partial}{\partial t}(x_i\rho_i) + \nabla\cdot(x_i\rho_i\mathbf{u}) - Q_i = 0, \quad i = 1,2,\ldots,\mathcal{N}_c, \tag{1}$$

where $t, \mathbf{u}$ and Q_i are the time, velocity vector and mass source term, respectively, and ρ_i is the density of component i. In Eq. (1), x_i is the mass fraction of component i, where $i = 1,2,\ldots,\mathcal{N}_c$, and $\mathcal{N}_c$ denotes the number of components, which is subject to the following constraint:

$$\sum_{i=1}^{\mathcal{N}_c} x_i = 1. \tag{2}$$

The equations of motion of a compressible viscous fluid may be written as:

$$\frac{\partial}{\partial t}(\rho\mathbf{u}) + \nabla\cdot(\rho\mathbf{u}\mathbf{u}) = \nabla\cdot\bar{\bar{\sigma}} - \nabla p + \rho g\mathbf{k}, \tag{3}$$

where $\bar{\bar{\sigma}}$ is the deviatoric stress tensor, p is the pressure, the bulk density is $\rho = \sum_i^{\mathcal{N}_c} x_i\rho_i$, g is the gravitational acceleration, and $\mathbf{k}$ is a unit vector pointing in the direction of gravity. Assuming $Q_i = 0$, testing with control volume basis functions M_m, and applying integration by parts and using the θ-time stepping method for the advection terms, Eq. (1) can be expressed as:

$$\int_{V_m} M_m\left(\frac{x_{im}^{n+1}\rho_{im}^{n+1} - x_{im}^{n}\rho_{im}^{n}}{\Delta t}\right)dV + \int_{\Gamma_m}\Big[\theta_i^{n+\frac{1}{2}}x_i^{n+1}\rho_i^{n+1}\mathbf{n}\cdot\mathbf{u}^{n+1} + \left(1-\theta_i^{n+\frac{1}{2}}\right)x_i^{n}\rho_i^{n}\mathbf{n}\cdot\mathbf{u}^{n}\Big]d\Gamma = 0, \quad m = 1,2,\ldots,\mathcal{M}, \tag{4}$$

where $\theta(\in\{0,1\})$ is the implicitness parameter, $\mathbf{n}$ is the outward-pointing unit normal vector to the surface of the control volume m, $\mathcal{M}$ is the number of control volumes, n represents the time level; here, V_m and Γ_m represent the volume and surface area of the control volume m, respectively. Dividing Eq. (4) by ρ_{im}^{n+1} and then summing over all components leads to the global mass conservation:

$$\int_{\Gamma_m}\Big[\Theta_m^{n+\frac{1}{2}}\mathbf{n}\cdot\mathbf{u}^{n+1} + (1-\Theta)_m^{n+\frac{1}{2}}\mathbf{n}\cdot\mathbf{u}^{n}\Big]d\Gamma = \int_{V_m} M_m\mathcal{S}_m^{n+\frac{1}{2}}dV, \quad m = 1,2,\ldots,\mathcal{M}. \tag{5}$$

Eq. (5) is also bounded by the component-mass constraints:

$$\sum_{i=1}^{\mathcal{N}_c} x_{im}^{n} = \sum_{i=1}^{\mathcal{N}_c} x_{im}^{n+1} = 1, \tag{6}$$

and the absorption term $\mathcal{S}_m^{n+\frac{1}{2}}$ is:

$$\mathcal{S}_m^{n+\frac{1}{2}} = -w_c\frac{1}{\Delta t}\left(1 - \sum_{i=1}^{\mathcal{N}_c} x_{im}^{n+1}\right) - \sum_{i=1}^{\mathcal{N}_c}\left(\frac{x_{im}{}^{n+1}\rho_{im}^{n+1} - x_{im}^{n}\rho_{im}^{n}}{\rho_{im}^{n+1}\Delta t}\right). \tag{7}$$

The term $w_c(\in\{0,1\})$ helps enforcing the component-mass constraint Eq. (6): $w_c = 1$ represents a full correction but may lead to an unstable scheme, whereas $w_c = 0$ represents a no-correction operation. Here, a compromise $w_c = 0.5$ is used. So, the first term in the *rhs* of Eq. (7) applies the summation constraint Eq. (6, as $w_c \to 1$) and effectively replaces the summation of the time implicit term on the *rhs* of Eq. (4) with $1/\Delta t$. By ensuring positivity of the effective absorption in the mass conservation associated with the w_c term, the scheme's stability may be improved. This means that the first term on the *rhs* of Eq. (7) is replaced with:

$$-w_c\frac{1}{\Delta t}\max\left\{1 - \sum_{i=1}^{\mathcal{N}_c} x_{im}^{n+1}, 0\right\}.$$

The space/time flux-limiting functions (from Eq. (5)) are defined as:

Please cite this article in press as: Pavlidis, D., et al. Two- and three-phase horizontal slug flow simulations using an interface-capturing compositional approach. Int. J. Multiphase Flow (2014), http://dx.doi.org/10.1016/j.ijmultiphaseflow.2014.07.007

$$\Theta_m^{n+\frac{1}{2}} = \sum_{i=1}^{\mathcal{N}_c} \theta_i^{n+\frac{1}{2}} \chi_i^{n+1} \left(\frac{\rho_i^{n+1}}{\rho_i^{n+1}{}_m} \right), \tag{8}$$

and

$$(1-\Theta)_m^{n+\frac{1}{2}} = \sum_{i=1}^{\mathcal{N}_c} \left(1-\theta_i^{n+\frac{1}{2}}\right) \chi_i^{n} \left(\frac{\rho_i^{n}}{\rho_i^{n+1}{}_m} \right). \tag{9}$$

The initial estimate of these flux-limiting functions in a time step are: $\Theta_m^{n+\frac{1}{2}} = 1$ and $(1-\Theta)_m^{n+\frac{1}{2}} = 0$.

A transient, mixed, finite element formulation is used to discretise the momentum equations (Eq. 3). A control volume discretisation of the continuity equations and a linear discontinuous Galerkin (Cotter et al., 2009a; Xiao et al., 2013) discretisation of the momentum equations are employed with backward Euler time stepping. Within each time step, the equations are iterated upon using a projection-based pressure determination method until all equations are simultaneously balanced.

In the mixed formulation, the domain is discretised into triangular or tetrahedral elements and in this work, they are P_1DG-P_2 elements (linear discontinuous between elements in velocity and quadratic continuous between elements in pressure). Fig. 1 shows the locations of the degrees of freedom for the P_1DG-P_2 element and the boundaries of the control volumes. A non-linear Petrov–Galerkin method is used to stabilise the momentum equations. This involves the addition of a non-linear diffusion term over and above the discretisation that results from a standard Bubnov–Galerkin discontinuous Galerkin discretisation (see Hughes and Mallet, 1986; Pain et al., 2001; Fang et al., 2013; Xie et al., 2014).

Method validation: collapsing water column test case

The model is evaluated using a collapsing water column test case in two spatial dimensions. The dimensions of the computational domain are 1 m × 1 m. The dimensions of the water column at time $t = 0$ s are 0.25 m × 0.5 m, in the x and y directions, respectively. The column is placed on the bottom-left corner of the domain. The acceleration due to gravity, which acts in the negative y direction, is 9.81 m/s^2. The two fluids, air and water, are assumed to be inviscid and their densities are 1 kg/m^3 and 1000 kg/m^3, respectively. Free-slip boundary conditions are applied on the sides and bottom of the domain. The top boundary is assumed to be open and a zero pressure condition is applied. The two-fluid volume fraction components are also prescribed on the top boundary (zero for the water, unity for the air). All boundary conditions are enforced weakly via surface integrals. A simple adaptive time stepping scheme is used to ensure that the Courant number (defined as $\Delta t \mathbf{J}^{-1}\mathbf{u}$, where $\mathbf{J}$ is the finite element Jacobian matrix) is under 0.1. One simulation is performed using a structured mesh with 100 equally-spaced layers in each direction.

In order to assess the many-material capability of the numerical approach, the water column is composed of four equally-sized components/materials of identical material properties. Therefore, in total, five materials, four components in the liquid phase in addition to air, are used in this test case. The initial condition for the numerical simulation of the collapsing multi-component water column is shown in the top-left panel of Fig. 2 while the remaining panels of this figure depict column collapse over a duration of 0.46 s and demonstrate that the interfaces separating all the components remain sharp at all times.

In order to perform detailed, quantitative comparisons with experimental data, the evolution of the non-dimensional column height and position of the leading edge in time are used as diagnostics. These are calculated by integrating the composition field on the left and bottom boundaries of the computational domain, for each diagnostic, respectively, for every time step. The water column height is non-dimensionalised by H the initial column height, the leading edge length is non-dimensionalised by W the initial column width to give y^* and x^*, respectively. The time for the column height plots is non-dimensionalised by $\sqrt{2g/H}$, while that for the leading edge length plots is non-dimensionalised by $\sqrt{2g/W}$ to give t_y and t_x, respectively.

The experimental results of Martin and Moyce (1952) are used as reference. One set of data for $W = 0.0572$ m (labelled as 'Experiment 1') is available for the column height, while two sets of data for $W = 0.0572$ m and $W = 0.0286$ m (labelled as 'Experiment 2') are available for the leading edge length. Comparison of the numerical results with the experimental data is shown in Fig. 3. As far as the water column height is concerned, the results from the numerical simulation are in good agreement with the experimental data (see Fig. 3, left). Regarding the leading edge comparisons, it is worth noting that the dam cannot be removed instantaneously in the experiments leading to a small time lag in the experimental data. This is evident in the comparisons presented in right panel of Fig. 3 and explains the systematic over-prediction of the data by the numerical predictions (Greaves, 2006). Nevertheless, despite this discrepancy, it can be concluded that the numerical results are in good agreement with experimental data. In addition, the results demonstrate the ability of the model to simulate multi-component, highly turbulent flows.

Numerical simulation of two-phase horizontal slug flow

The model is used to carry out two-dimensional simulations of horizontal two-phase slug flows; here, the two phases are air and water with the same properties as those mentioned in the previous section. The dimensions of the computational domain are

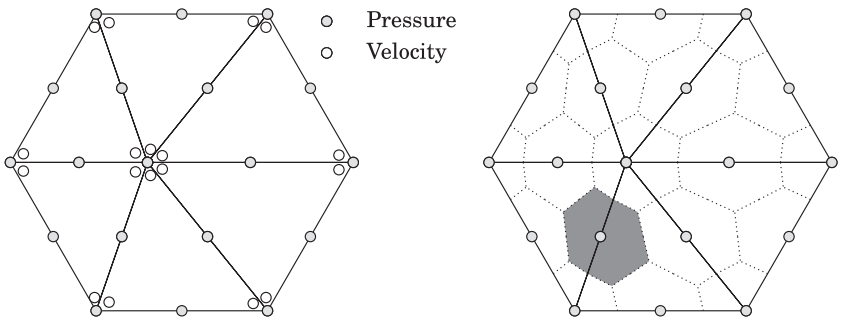

Fig. 1. Finite elements used to discretise the spatial derivatives in the governing equations are shown in the left panel. The central position of key solution variables are indicated here for the P_1DG-P_2 element pair. A diagram showing the relationship between the intersecting control volumes (dashed lines) and elements for the P_2 element is shown in the right panel.

Please cite this article in press as: Pavlidis, D., et al. Two- and three-phase horizontal slug flow simulations using an interface-capturing compositional approach. Int. J. Multiphase Flow (2014), http://dx.doi.org/10.1016/j.ijmultiphaseflow.2014.07.007

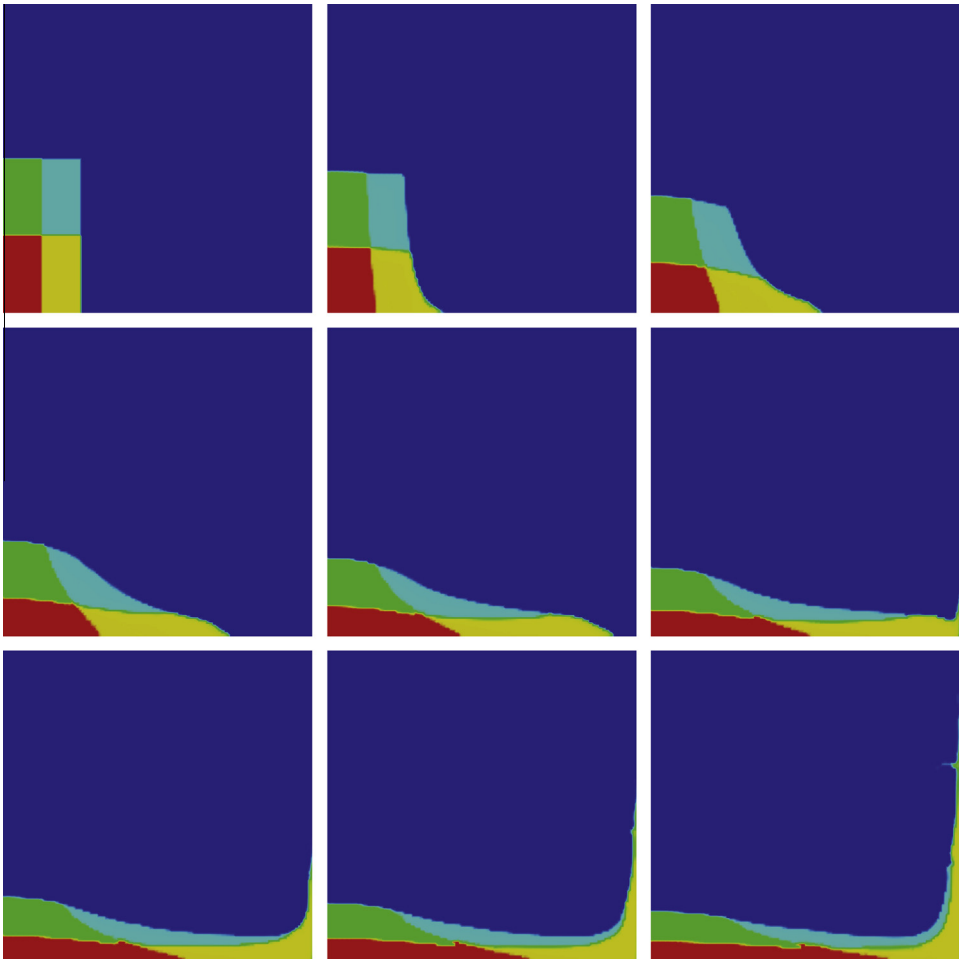

Fig. 2. Numerical simulation of a collapsing column comprising five materials shown in red, yellow, light blue, and green for the liquid phases, dark blue for air at nine time levels: from top-left to bottom-right, the time t is $\approx$ 0, 0.1, 0.18, 0.25, 0.31, 0.35, 0.38, 0.41 and 0.46 s, respectively. (For interpretation of the references to colour in this figure legend, the reader is referred to the web version of this article.)

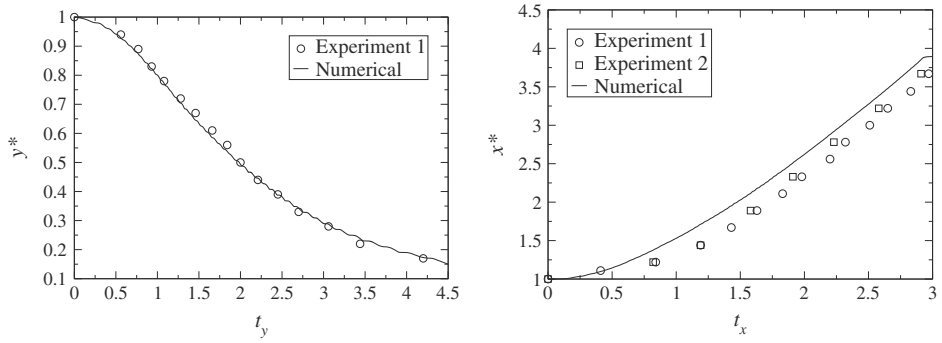

Fig. 3. Comparison of the results obtained from the numerical simulation of a multi-component collapsing water column with experimental data from Martin and Moyce (1952) in terms of temporal evolution of the non-dimensional column height, y^*, and leading edge, x^* (see text for definitions of scalings), shown in the left and right panels, respectively.

6 m $\times$ 0.1 m, and the flow is initially stratified, with water occupying the bottom half of the domain. The acceleration due to gravity is 9.81 m/s^2 and gravity acts on the y direction.

Air is injected into the domain from the top half of the left boundary with a 5 m/s uniform velocity. Water is injected into the domain from the bottom half of the left boundary and a number of simulations with different uniform water inflow velocities (0.5–1.5 m/s) are undertaken. It is worth noting that for velocities smaller than $\approx$1 m/s, a wavy stratified flow, but not slug flow, is reproduced by the model, which is expected based on previous experimental results (Mandhane et al., 1974). Results associated with a water inlet velocity of 1.5 m/s are presented here.

Free-slip boundary conditions are applied on the top and bottom boundaries of the domain. This approach is employed to avoid having to resolve the near-wall region. The right boundary is assumed to be open and the hydrostatic pressure is prescribed. The two phase volume fractions are also prescribed on the left

Please cite this article in press as: Pavlidis, D., et al. Two- and three-phase horizontal slug flow simulations using an interface-capturing compositional approach. Int. J. Multiphase Flow (2014), http://dx.doi.org/10.1016/j.ijmultiphaseflow.2014.07.007

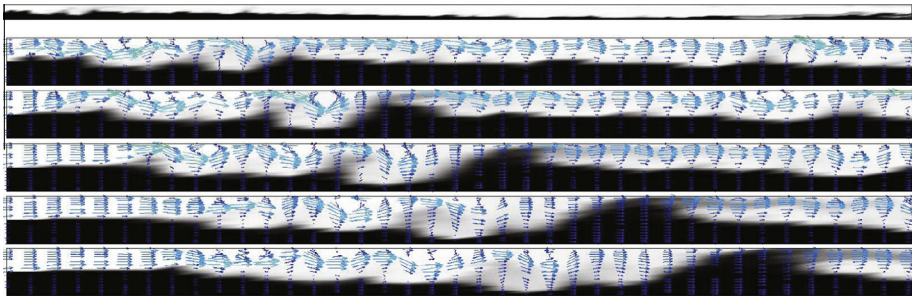

Fig. 4. Numerical simulation of air–water slug flow in a rectangular channel generated with uniform inlet velocities of 1.5 m/s and 5 m/s for the water and air phases, respectively. The panels depict snapshots of the volume fraction fields in which the air and water phases are shown in white and black, respectively. The top panel shows the entire computational domain at $t \approx 5$ s, while the remaining panels show the development of a slug near the channel inlet at time intervals of 6.25×10^{-2} s starting from $t \approx 5$ s. Velocity vectors are also shown in the slug development panels.

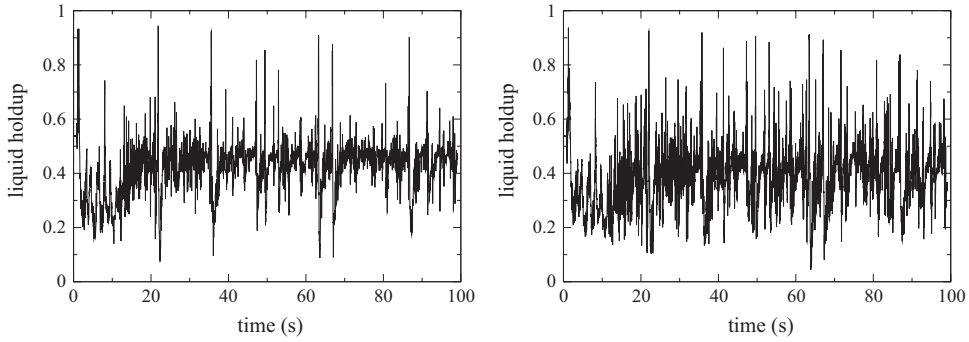

Fig. 5. Numerical simulation of air–water slug flow in a rectangular channel generated with uniform inlet velocities of 1.5 m/s and 5 m/s for the water and air phases, respectively. The panels show the evolution of the non-dimensional water phase volume fraction integral over a vertical line (liquid holdup) with time 5 m (left) and 5.75 m (right) from the inflow boundary. Data points are calculated every 25 time steps.

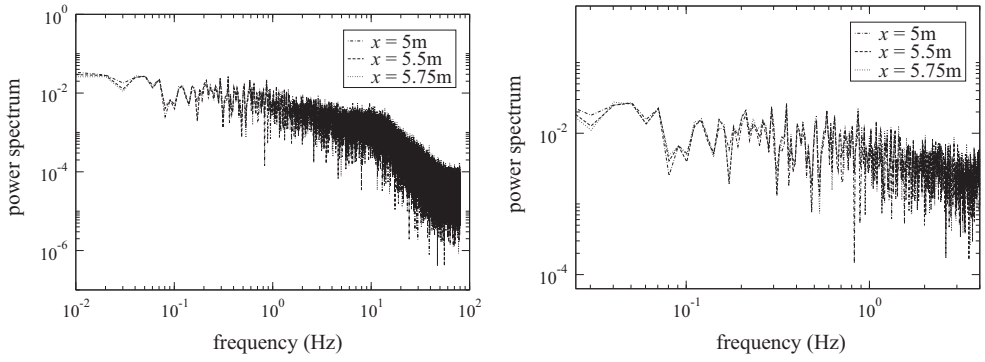

Fig. 6. Numerical simulation of air–water slug flow in a rectangular channel generated with uniform inlet velocities of 1.5 m/s and 5 m/s for the water and air phases, respectively. The panels show power spectra produced by liquid holdup time series, such as those presented in Fig. 5, for distances 5 m, 5.5 m and 5.75 m from the inflow boundary. The whole spectrum for the three time series is shown in the left panel. The right panel focuses around frequencies between 0.1 Hz and 1 Hz. Three peaks at 0.22, 0.29 and 0.35 are evident for all three locations; these are the slugging frequencies.

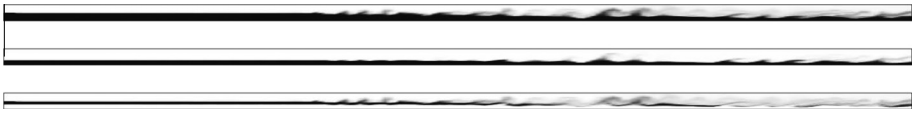

Fig. 7. Numerical simulation of air–water–oil slug flow in a rectangular channel generated with uniform inlet velocities of 1.5 m/s and 5 m/s for the liquid (water and oil) and air phases, respectively. The panels depict snapshots of the volume fraction fields at time $t \approx 7$ s. The top panel shows the combined water and oil volume fraction in black. The middle panel shows the water volume fraction in black and the bottom panel shows the oil volume fraction in black. Air is represented by white in all panels. The entirety of the computational domain is shown here.

and right boundaries based on the initial condition (stratified). All boundary conditions are enforced weakly via the use of surface integrals. A simple adaptive time stepping scheme is used to ensure that the Courant number (defined as $\Delta t \mathbf{J}^{-1}\mathbf{u}$, where $\mathbf{J}$ is the finite element Jacobian matrix) is under 0.5. One simulation is performed using a structured mesh with 150 and 18 layers in

Please cite this article in press as: Pavlidis, D., et al. Two- and three-phase horizontal slug flow simulations using an interface-capturing compositional approach. Int. J. Multiphase Flow (2014), http://dx.doi.org/10.1016/j.ijmultiphaseflow.2014.07.007

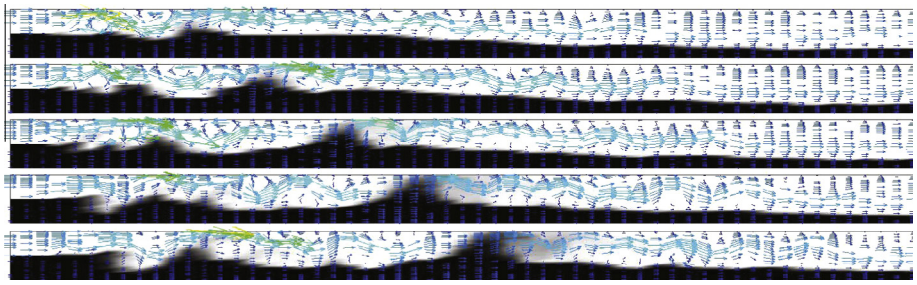

Fig. 8. Numerical simulation of air–water–oil slug flow in a rectangular channel generated with uniform inlet velocities of 1.5 m/s and 5 m/s for the liquid (water and oil) and gas (air) phases, respectively. The panels depict snapshots of the volume fraction fields in which the gas and combined liquid (water and oil) phases are shown in white and black, respectively. Velocity vectors are also shown here. The development of a slug near the channel inlet at time intervals of 6.25×10^{-2} s starting from $t \approx 4$ s is shown here.

the horizontal and vertical directions, respectively. The layers are equally-spaced in the horizontal, while they are more densely packed near the top and bottom boundaries in the vertical direction. Preliminary trials suggest that this resolution is sufficient to capture slugging.

In Fig. 4 snapshots of the volume fraction fields together with velocity vectors at various stages of the simulated two-phase flow are shown. The top panel in Fig. 4 depicts the entire computational domain at $t \approx 5$ s, while the remaining five panels, from top to bottom, show the spatio-temporal development of a slug near the inflow boundary every 6.25×10^{-2} s starting from $t \approx 5$ s. It can be seen that the liquid velocity decreases and so the water level increases at that region until it reaches the top boundary. At that point, the flow is accelerated by the air and a slug is formed. It is worth noting that despite the high Reynolds number nature of the flow in both water and air, coherent vortex structures only appear in the gas phase and the velocity vectors in the liquid phase are generally aligned with the flow direction.

The diagnostic used to evaluate the ability of the numerical method to accurately predict two-phase horizontal slug flows is the slug frequency. A detailed review of the most fundamental two-phase slug frequency correlations and experimental data sets up to date can be found in Al-Safran (2009). For the parameter values that characterise the flow simulated here, the slug frequency is expected to be approximately equal to 0.26 Hz as predicted by all but the Gregory and Scott (1969) correlation (which predicts approximately 0.54 Hz); the latter, however, is unreliable for the channel dimensions considered here. The slug frequency predicted by the numerical simulation evaluated 5 m from the inflow boundary is ≈0.3 Hz, which is in good agreement with the experimentally-determined correlations.

The evolution of the non-dimensional water phase volume fraction integral over a vertical line (liquid holdup) with time 5 m and 5.75 m from the inflow boundary is shown in Fig. 5. Integrals are calculated using the computational mesh (19 points). Data points (liquid holdup) are calculated every 25 time steps. The power spectra, obtained by performing discrete Fourier transforms, of these time series, plus one more 5.5 m from the inflow boundary, are shown in Fig. 6. The whole spectrum for the three time series is shown along with a zoom-in around the 0.1–1 Hz frequency band. Power spectra for lower frequencies are unreliable since the simulation was run for ≈100 s. Three peaks at 0.22, 0.29 and 0.35 are

Fig. 9. Numerical simulation of air–water–oil slug flow in a rectangular channel generated with uniform inlet velocities of 1.5 m/s and 5 m/s for the liquid (water and oil) and gas (air) phases, respectively. The panels depict snapshots of the volume fraction fields in which the water and combined air and oil phases are shown in black and white, respectively. The development of a slug near the channel inlet at time intervals of 6.25×10^{-2} s starting from $t \approx 4$ s is shown here.

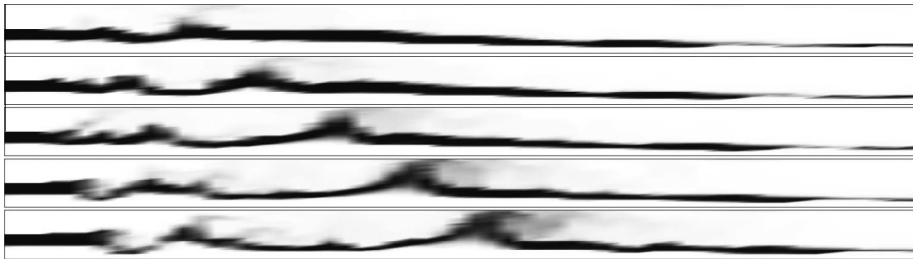

Fig. 10. Numerical simulation of air–water–oil slug flow in a rectangular channel generated with uniform inlet velocities of 1.5 m/s and 5 m/s for the liquid (water and oil) and gas (air) phases, respectively. The panels depict snapshots of the volume fraction fields in which the oil and combined air and water phases are shown in black and white, respectively. The development of a slug near the channel inlet at time intervals of 6.25×10^{-2} s starting from $t \approx 4$ s is shown here.

Please cite this article in press as: Pavlidis, D., et al. Two- and three-phase horizontal slug flow simulations using an interface-capturing compositional approach. Int. J. Multiphase Flow (2014), http://dx.doi.org/10.1016/j.ijmultiphaseflow.2014.07.007

evident for all three locations; these correspond to the slugging frequencies.

Based on the above discussion, the simulation results are qualitatively consistent with experimental observations in terms of spatio-temporal development of slug, and compare well quantitatively with existing correlations in terms of slug frequencies. Having developed confidence in the reliability of the numerical method, it is now applied to three-phase slug flow simulations; the results of these simulations are presented next.

Numerical simulation of three-phase horizontal slug flow

The model is used to simulate horizontal three-phase (air–water–oil) slug flows in two dimensions. The dimensions of the computational domain are 6 m $\times$ 0.1 m. The flow is initially stratified, with water occupying the bottom quarter of the domain, air occupying the top half of the domain and oil occupying the remaining space. The acceleration due to gravity is 9.81 m/s^2 and gravity acts on the y direction. The three fluids' (air, water and oil) dynamic viscosities are 10^{-5}, 10^{-3} and 10^{-3} kg/(m s) and their densities are 1, 1000 and 800 kg/m^3, respectively.

Snapshots of the liquid volume fraction fields at time $t \approx 7$ s of the simulated three-phase flow are shown in Fig. 7. The entirety of the computational domain is shown here.

In Fig. 8 snapshots of the volume fraction fields together with velocity vectors at various stages of the simulated three-phase flow are shown. The five panels, from top to bottom, show the spatio-temporal development of a slug near the inflow boundary every 6.25×10^{-2}s starting from $t \approx 4$ s. The two liquid (water and oil) phases are shown in black, while the gas (air) phase is shown in white. Figs. 9 and 10 show the two liquid phases' volume fraction fields separately for the five time levels shown in Fig. 8. The water phase is shown in Fig. 9, while the oil phase is shown in Fig. 10. The results presented in this section are preliminary. Long-time simulations will be carried out and their results will be compared against experimental data (Lee et al., 1993; Hall, 1997) in terms of flow structure as well as slug frequencies.

Conclusions

A novel method for simulating slug flows of arbitrary number of phases has been presented. The method is based on a mixed control volume-finite element method multi-component formulation and the P_1DG-P_2 (linear velocity, discontinuous between elements and quadratic pressure, continuous between elements) element pair. The compositional approach embeds interface information into the continuity equations. A novel interface-capturing scheme based on high-order accurate compressive advection methods is used. The main advantages of this method over existing ones are that arbitrary numbers of phases, with arbitrary equations of state, can be naturally modelled and that key balances (buoyancy force and pressure gradient here) are enforced exactly (no spurious velocities are generated when used with unstructured meshes).

The numerical method was initially evaluated using a five-material collapsing water column test case. Evolution of the water column height and leading edge length with time was in good agreement with experimental results. In addition, interfaces between the five materials were sharp. The method was then used to simulate two- and three-phase horizontal slug flows. The two-phase slugging results were qualitatively and quantitatively in good agreement with experimental data and well-established correlations. The preliminary three-phase slugging results were qualitatively in good agreement with experimental data; quantitative comparisons will be carried out in the future. Future work will also include the application of the method for the three-dimensional simulation of three-phase slug flows using fully-unstructured adaptive meshes (see Xie et al., 2014).

Acknowledgements

The authors would like to thank the EPSRC MEMPHIS multiphase programme Grant (EP/K003976/1), the EPSRC computational modelling for advanced nuclear power plants project and the EU FP7 projects THINS and GoFastR for helping to fund this work.

References

Al-Safran, E., 2009. Investigation and prediction of slug frequency in gas/liquid horizontal pipe flow. J. Petrol. Sci. Eng. 69, 143–155.
Cotter, C.J., Ham, D.A., Pain, C.C., 2009a. A mixed discontinuous/continuous finite element pair for shallow-water ocean modelling. Ocean Model. 26, 86–90.
Cotter, C.J., Ham, D.A., Pain, C.C., Reich, S., 2009b. LBB stability of a mixed Galerkin finite element pair for fluid flow simulations. J. Comput. Phys. 228, 336–348.
Darwish, M., Moukalled, F., 2003. The χ-schemes: a new consistent high-resolution based on the normalised variable methodology. Comp. Meth. Appl. Mech. Eng. 192, 1711–1730.
Darwish, M.S., 1993. A new high-resolution scheme based on the normalized variable formulation. Numer. Heat Transfer – Part B 24, 353–371.
de Cachard, F., Delhaye, J.M., 1996. A slug-churn flow model for small-diameter airlift pumps. Int. J. Multiph. Flow 22, 627–649.
Fabre, J., Line, A., 1992. Modelling of two-phase slug flow. Ann. Rev. Fluid Mech. 24, 21–46.
Fang, F., Pain, C.C., Navon, I.M., ElSheikh, A.H., Du, J., Xiao, D., 2013. Non-linear Petrov–Galerkin methods for reduced order hyperbolic equations and discontinuous finite element methods. J. Comput. Phys. 234, 540–559.
Fernandes, R.C., Semiat, R., Dukler, A.E., 1983. Hydrodynamic model for gas–liquid slug flow in vertical tubes. Am. Inst. Chem. Eng. J. 29, 981–989.
Greaves, D.M., 2006. Simulation of viscous water column collapse using adapting hierarchical grids. Int. J. Numer. Meth. Fluids 50, 693–711.
Gregory, G., Scott, D., 1969. Correlation of liquid slug velocity and frequency in horizontal co-current gas–liquid slug flow. Am. Inst. Chem. Eng. J. 15, 933–935.
Hall, A.W.R., 1997. Flow pattern in three-phase gas flows of oil, water and gas. In: Proceedings of the 8th International Conference on Multiphase Production. Cannes, France.
Hughes, T.J.R., Mallet, M., 1986. A new finite element formulation for computational fluid dynamics – IV. A discontinuity-capturing operator for multi-dimensional advection–diffusion systems. Comp. Meth. Appl. Mech. Eng. 58, 329–336.
King, M.J.S., Hale, C.P., Lawrence, C.J., Hewitt, G.F., 1998. Characteristics of flow rate transients in slug flow. Int. J. Multiph. Flow 24, 825–854.
Lee, A.-H., Sun, J.-Y., Jepson, W.P., 1993. Study of flow regime transitions of oil–water–gas mixtures in horizontal pipelines. In: Proceedings of the 3rd International Offshore and Polar Engineering Conference. Singapore.
Leonard, B.P., 1991. The ULTIMATE conservative difference scheme applied to unsteady one-dimensional advection 88, 17–74.
Mandhane, J.M., Gregory, G.A., Aziz, K., 1974. A flow pattern map for gas–liquid flow in horizontal pipes. Int. J. Multiph. Flow 1, 537–553.
Martin, J.C., Moyce, W.J., 1952. An experimental study of the collapse of liquid columns on a rigid horizontal plane. Philos. Trans. Royal Soc. Lond., Ser. A 244, 312–324.
Omebere-Iyari, N.K., Azzopardi, B.J., Ladam, Y., 2007. Two-phase flow patterns in large diameter vertical pipes at high pressures. Am. Inst. Chem. Eng. J. 53, 2493–2504.
Pain, C.C., de Oliveira, C.R.E., Goddard, A.J.H., Umpleby, A.P., 2001. Criticality behaviour of dilute plutonium solutions. Nucl. Sci. Technol. 30, 194–214.
Ujang, P.M., Lawrence, C.J., Hale, C.P., Hewitt, G.F., 2006. Slug initiation and evolution in two-phase horizontal flow. Int. J. Multiph. Flow 32, 527–552.
Wilson, C., 2009. Modelling Multiple-Material Flows on Adaptive Unstructured Meshes. Ph.D. thesis, Department of Earth Science and Engineering, Imperial College London.
Xiao, D., Fang, F., Du, J., Pain, C.C., Navon, I.M., Buchan, A.G., ElSheikh, A.H., Hu, G., 2013. Non-linear Petrov–Galerkin methods for reduced order modelling of the Navier–Stokes equations using a mixed finite element pair. Comp. Meth. Appl. Mech. Eng. 255, 147–157.
Xie, Z., Pavlidis, D., Percival, J.R., Gomes, J.L.M.A., Pain, C.C., Matar, O.K., 2014. Adaptive unstructured mesh modelling of multiphase flows. Int. J. Multiph. Flow (submitted for publication).

Please cite this article in press as: Pavlidis, D., et al. Two- and three-phase horizontal slug flow simulations using an interface-capturing compositional approach. Int. J. Multiphase Flow (2014), http://dx.doi.org/10.1016/j.ijmultiphaseflow.2014.07.007